Biosensors and Bioelectronics 24 (2008) 644–649

Contents lists available at ScienceDirect

Biosensors and Bioelectronics

journal homepage: www.elsevier.com/locate/bios

Biofunctional nanocomposite of carbon nanofiber with water-soluble porphyrin for highly sensitive ethanol biosensing

Lina Wu[a], Jianping Lei[a,*], Xueji Zhang[b], Huangxian Ju[a,*]

[a] Key Laboratory of Analytical Chemistry for Life Science (Ministry of Education of China), Department of Chemistry, Nanjing University, Nanjing 210093, PR China
[b] Department of Chemistry, University of South Florida, 4202 East Fowler Avenue, CHE 305, Tampa, FL 33620-5250, USA

ARTICLE INFO

Article history:
Received 20 February 2008
Received in revised form 6 June 2008
Accepted 9 June 2008
Available online 17 June 2008

Keywords:
Nanocomposite
Biosensors
Carbon nanofiber
Water-soluble porphyrin
Alcohol oxidase
Ethanol

ABSTRACT

A biofunctional hybrid nanocomposite of carbon nanofiber (CNF) with water-soluble iron(III) meso-tetrakis(*N*-methylpyridinum-4-yl) porphyrin (FeTMPyP) was designed via non-covalent interaction for preparation of highly sensitive ethanol biosensor. The prepared nanocomposite showed good dispersion in water and was characterized with steady-state electronic absorption spectroscopy and scanning electron microscope. The nanocomposite combined the good conductivity of CNF and the excellent catalytic activity of both CNF and FeTMPyP toward the reduction of dissolved oxygen, producing a method for amperometric detection of oxygen ranging from 6.5 nM to 6.4 μM at a low overpotential. The nanocomposite modified electrode was further used for assembly of alcohol oxidase to construct an amperometric biosensor for ethanol. The biosensor showed rapid and highly sensitive response to ethanol with a linear range from 2.0 μM to 112 μM. The immobilized alcohol oxidase also showed its direct electrochemistry. The biofunctional nanocomposite provides a new way to not only construct the highly sensitive biosensors but also mimic the catalytic activity of enzyme in the life process.

1. Introduction

Porphyrins are important classes of conjugated organic molecules, which mimic the active site of many important enzymes such as hemoglobin, myoglobin, cytochrome c oxidase, nitric oxide reductase, vitamin B_{12}, and chlorophyll (Collman et al., 2004; Balaban et al., 2005; Wasser et al., 2005). Iron-porphyrin tightly correlating with heme-containing proteins has excellent electrocatalytic properties toward the detection of many biochemical analytes, such as nitric oxide (Lei et al., 2004a), O_2 (Liu et al., 2007), nitrite (Lei et al., 2004b), sulfite (Li et al., 2003), bromate, iodate and chlorate (Salimi et al., 2007). However, most of them focus on disordered porphyrin dissolved in solution or immobilized in polymer film. With the great progress made in nanoscience and nanotechnology, interest has been increasing in exploring the orderly assembly of porphyrin with various nanostructures including semiconductor TiO_2, CdSe quantum dots and carbon nanotubes (CNTs) (Murakami et al., 2003; Chen and Collier, 2005; Guldi et al., 2005; Zenkevich et al., 2005; Takagi et al., 2006). Especially, covalence and non-covalence interactions between the porphyrin and carbon nanotubes have extensively been investigated to build photovoltaic devices due to their unique photophysical and photochemical properties (Guldi et al., 2005). In fact, the functionalization of sidewalls of CNTs through non-covalence containing axial coordination and π–π interaction is an effective way for improving their dispersion or dissolution properties without changing of the sp^2 nanotube structure (Chen et al., 2001).

Compared with CNTs, carbon nanofiber (CNF) has larger surface-active groups-to-volume ratio (Vamvakaki et al., 2006), better mechanical stability (Cui et al., 2004), and easier mass production (Jang et al., 2005). Especially, CNF processes more edge sites on the out wall than CNTs. Based on these advantages, the acid-treated CNF as a biocompatible electron conductor has been used to construct a biosensor for dihydronicotinamide adenine dinucleotide (NADH) with a low oxidation overpotential and a sensitive impedance cell sensor (Hao et al., 2007; Wu et al., 2007a). This work further designed a orderly biofunctional hybrid nanocomposite of CNF with water-soluble enzyme model, iron(III) meso-tetrakis(*N*-methylpyridinum-4-yl) porphyrin (FeTMPyP) (inset in Fig. 1), to combine the good conductivity of CNF and the excellent catalytic activity of both CNF and FeTMPyP for sensitive biosensing of ethanol.

The measurement of trace ethanol plays an important role in different industries and biotechnological processes such as production of alcoholic beverages, foodstuffs, pharmaceutical products, and clinical and forensic analysis. Ethanol biosensors are commonly based on either alcohol dehydrogenase or alcohol oxidase (AOx)

* Corresponding authors. Tel.: +86 25 83593593.; fax: +86 25 83593593.
E-mail addresses: jpl@nju.edu.cn (J. Lei), hxju@nju.edu.cn (H. Ju).

0956-5663/$ – see front matter © 2008 Elsevier B.V. All rights reserved.
doi:10.1016/j.bios.2008.06.009

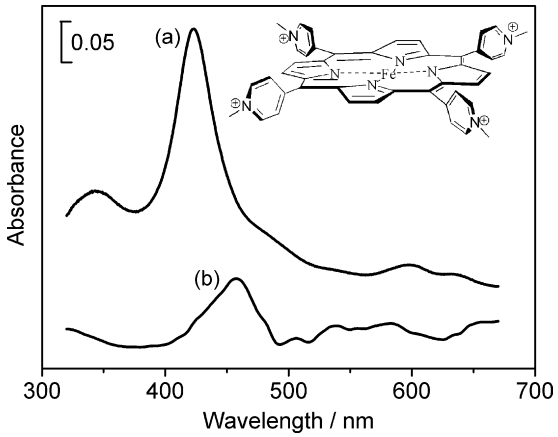

Fig. 1. Steady-state absorption spectra of 5 μM FeTMPyP (a) and 0.5 mg ml^{-1} CNF–FeTMPyP (b) in aqueous solution. Inset: Chemical structure of FeTMPyP.

(Boujtita et al., 2000; Gülce et al., 2002; Hasunuma et al., 2004; Wu and Choi, 2004; Akyilmaz and Dinçkaya, 2005; Azevedo et al., 2005; Yıldız and Toppare, 2006; Wen et al., 2007). The AOx-based ethanol biosensors use molecular oxygen to oxidize ethanol, and thus detect ethanol by monitoring O_2 consumption at −600 mV or H_2O_2 formation (Azevedo et al., 2005). The H_2O_2 formation can be detected by its oxidation at +600 mV or its reduction in presence of horseradish peroxidase (HRP). The latter is usually performed with bienzymatic sensors based on the co-immobilization of AOx with HRP. However, an appropriate mediator is currently required for accelerating the electron transfer between HRP and electrode. Based on the synergic catalytic ability of CNF and FeTMPyP toward reduction of O_2, we herein prepared a biofunctional nanocomposite, CNF–FeTMPyP, to act as both electron conductor and catalytic mediator for O_2 reduction, which could occur at −0.060 V, leading to a highly sensitive amperometric biosensor for ethanol. The detection could be performed at low reduction overpotential with convenient operation and acceptable stability. Thus the well-dispersed biofunctional hybrid nanocomposite is promising in constructing biosensors and mimicking the catalytic activity of enzyme for life science research.

2. Materials and methods

2.1. Material

CNF was a gift from WPI (Sarasota, USA). AOx (from *Hansenula polymorpha*, 20–40 U mg^{-1}) and poly(vinyl alcohol) (PVA) were purchased from Sigma. Water-soluble FeTMPyP was prepared according to the method reported previously (Pasternack et al., 1977; Bedioui et al., 1993) Other reagents were of analytical reagent grade. All solutions were prepared with twice-distilled water. The buffer for the assay was 0.2 M phosphate buffer saline (PBS), prepared by mixing stock standard solution of K_2HPO_4 and KH_2PO_4. The O_2-saturated standard solution was prepared for the amperometric experiments by bubbling double distilled water with pure O_2 at room temperature for 1 h, in which the O_2 concentration was 2.6×10^{-4} M calculated from its saturated solubility.

2.2. Preparation of AOx/CNF–FeTMPyP/GCE

The GCE was successively polished to a mirror finish using 0.3 μm and 0.05 μm alumina slurry (Beuhler) followed by rinsing thoroughly with twice-distilled water. After successive sonication in 1:1 nitric acid, acetone and twice-distilled water, the electrode was rinsed with twice-distilled water and allowed to dry at room temperature. This whole process could wash off the impurity adsorbed on the electrode surface. The assembly of CNF–FeTMPyP was achieved by adding 25 mg CNF to 5 ml of 2 mg ml^{-1} FeTMPyP solution and then sonicating for 30 s at room temperature, followed with vigorously vibrating for 30 min. The resulting suspension was then centrifuged for 10 min at 10,000 rpm to remove the free FeTMPyP. The obtained solid was resuspended in water with vigorously vibrating for 10 min and centrifuged again to wash out any unbound porphyrin. The as-prepared nanocomposite was resuspended in water for carrying out different experiments. 3.0 μl of CNF–FeTMPyP nanocomposite was dropped on a pretreated GCE and dried in a silica gel desiccator to obtain CNF–FeTMPyP modified electrode. 3.0 μl of 10 mg ml^{-1} AOx in PBS was dropped on the CNF–FeTMPyP modified electrode and dried in a silica gel desiccator for 30 min. Then 3.0 μl of 1% with poly(vinyl alcohol) solution was dropped on the membrane to obtain the amperometric biosensor for ethanol.

2.3. Apparatus

Electrochemical measurements were performed on a CHI 660 electrochemical analyser (Co. CHI, USA) with a conventional three-electrode system comprised of platinum wire as auxiliary, saturated calomel electrode as reference and the modified glassy carbon electrode (GCE) as working electrodes. The cyclic voltammetric and amperometric experiments were performed in a thermostated electrochemical cell at 25 °C. Amperometric experiments were carried out in an air-saturated 0.2 M pH 7.0 PBS by applying a potential step of −0.20 V. For morphological analysis, the sample films were prepared in the same way as those for voltammetric measurements on different slides dealt with nitric acid and the mixture of H_2SO_4 and H_2O_2 (1:1). After coated with Au film to improve the conductivity, these films were examined under SEM (SEM, LEO 1530 VP, Germany).

3. Results and discussion

3.1. Characterization of CNF–FeTMPyP

FeTMPyP is water-soluble cationic porphyrin with π–π conjugated macrocycle on the porphin ring (inset in Fig. 1). After CNF was added to FeTMPyP solution followed with sonication and vibrating, the interaction between FeTMPyP and CNF via non-covalent π–π stacking resulted in the formation of CNF–FeTMPyP nanocomposite. The formed hybrid nanocomposite showed good dispersion in water, and no precipitation of CNF was observed after the resulted suspension stored for three months. The formation could be demonstrated with steady-state electronic absorption spectroscopy and scanning electron microscope (SEM). The typical absorption spectrum of FeTMPyP showed an intense Q band absorption at 422 nm and two less intense Soret bands at 598 nm and 640 nm (curve a, Fig. 1). Compared to free FeTMPyP, the CNF–FeTMPyP showed more complicated absorption (curve b, Fig. 1). The Soret band was broadened and red-shifted from 422 nm to 458 nm, while two Q bands blue-shifted to 537 nm and 583 nm. More interestingly, a new peak clearly appeared at 506 nm, which was attributed to J-type aggregate of FeTMPyP nucleated on CNF (Chen and Collier, 2005). These results suggested that the CNF surface was responsible for assembling porphyrin in an orderly fashion (Hasobe et al., 2005), leading to the electronic communication between the two components, which was important fundamental for accelerating electron transfer and developing efficient photovoltaic devices and biosensors.

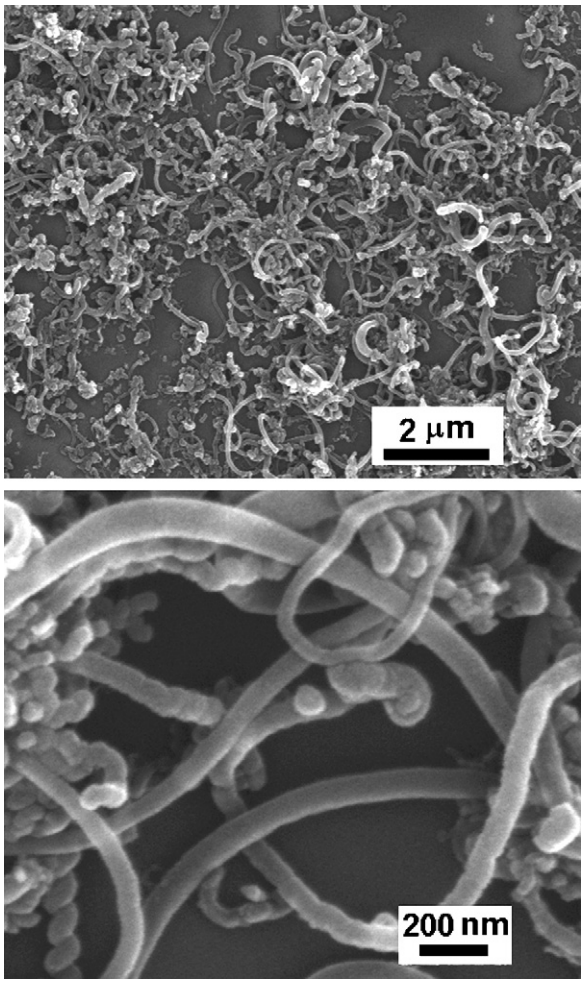

Fig. 2. Scanning electron micrographs of electrode coated with CNF–FeTMPyP at different amplifications.

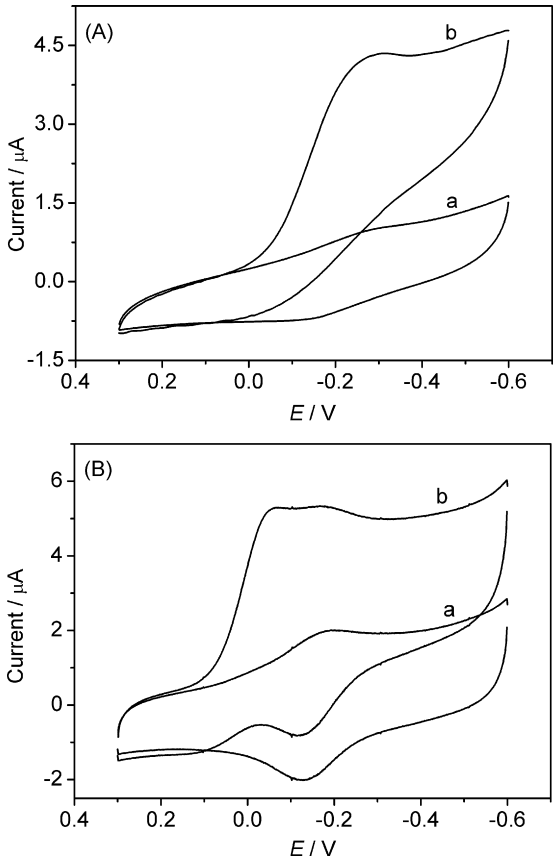

Fig. 3. Cyclic voltammograms of FeTMPyP (A) and CNF–FeTMPyP (B) modified GCE in nitrogen-saturated (a) and air-saturated (b) pH 7.0 0.2 M PBS. Scan rate: 0.01 V s^{-1}.

From the SEM image of CNF–FeTMPyP nanocomposite its diameter was in the range of 30–50 nm (Fig. 2), which was similar to that of CNF used in our previous works (Hao et al., 2007; Wu et al., 2007a). Thus the assembly of FeTMPyP on CNF did not obviously increase the size of CNF. However, the SEM image showed good dispersion of the hybrid nanoparticle on sampling support due to its high solubilization in aqueous solution, suggesting that the CNF surface was covered by cationic FeTMPyP. This homogeneous and porous nanostructure provided a significant increase of effective electrode surface for loading of biomolecules.

3.2. Voltammetric behavior of nanocomposite and optimization condition for its preparation

The cyclic voltammogram of FeTMPyP modified electrode in oxygen-free pH 7.0 PBS showed a couple of weak redox peaks at −0.263 V and −0.149 V (ΔE_p = 114 mV) at 0.01 V s^{-1}, while the redox peaks of the immobilized CNF–FeTMPyP occurred at −0.184 V and −0.130 V (ΔE_p = 54 mV) (curve a, Fig. 3). These peaks were attributed to the direct electron transfer between FeTMPyP and electrode. The decrease of ΔE_p indicated the formation of hybrid nanocomposite led to faster electron transfer rate due to the presence of CNF, which was consistent with the result of steady-state electronic absorption spectroscopy.

In air-saturated pH 7.0 PBS the cyclic voltammogram of FeTMPyP modified electrode showed the electrocatalytic ability towards reduction of dissolved oxygen, which resulted in dramatic increase of the reduction peak of FeTMPyP and decrease in the oxidation peak (curve b, Fig. 3A). In comparison of Fig. 3B(a) with Fig. 3B(b) the reduction of oxygen proceeded along with the reduction of Fe^{III}TMPyP. The dramatic increase of the reduction peak of FeTMPyP at CNF–FeTMPyP modified electrode also showed a typical EC catalytic regeneration mechanism (Bard and Faulkner, 2001). This could be demonstrated from the cyclic voltammogram of CNF–FeTMPyP modified electrode in oxygen-saturated solution, in which the oxidation peak disappeared. The appearance of oxidation peak of FeTMPyP in Fig. 3B(b) was due to the low oxygen concentration in solution and high content of FeTMPyP in CNF–FeTMPyP nanocomposite. The electrocatalytic reduction of dissolved oxygen at CNF–FeTMPyP modified electrode started at the potential of about +0.150 V, close to its physiological reduction potential in biological systems (Boultatov et al., 2002), and the reduction peak occurred at −0.060 V, which was more positive than those of −0.278 V at FeTMPyP modified electrode and −0.310 V at an acid-treated CNF modified electrode (Wu et al., 2007b). Thus, the CNF–FeTMPyP nanocomposite had a synergy effect of CNF and FeTMPyP for electrocatalyzing or accelerating the reduction of dissolved oxygen.

In order to obtain excellent performance for analytical purpose, the preparation of CNF–FeTMPyP nanocomposite was firstly optimized. At the FeTMPyP concentration of 2 mg ml^{-1}, with increasing amount of CNF mixed in the solution for preparation of the nanocomposite, the electrocatalytic reduction potential of dissolved oxygen shifted positively and peak current increased. At the amount of 5 mg CNF mixed in 1.0 ml FeTMPyP solution the reduction potential reached the most positive value, and the reduc-

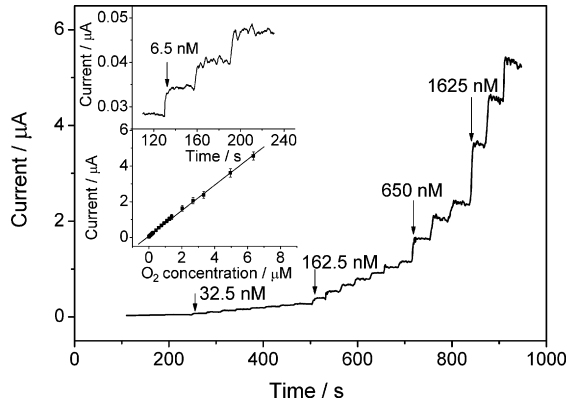

Fig. 4. Typical steady-state current response of the CNF–FeTMPyP modified electrode to successive addition of different volumes of oxygen-saturated solution into nitrogen-saturated pH 7.0 0.2 M PBS. Applied potential, −0.20 V. Upper inset: Amplified response curve. Lower inset: Calibration curve.

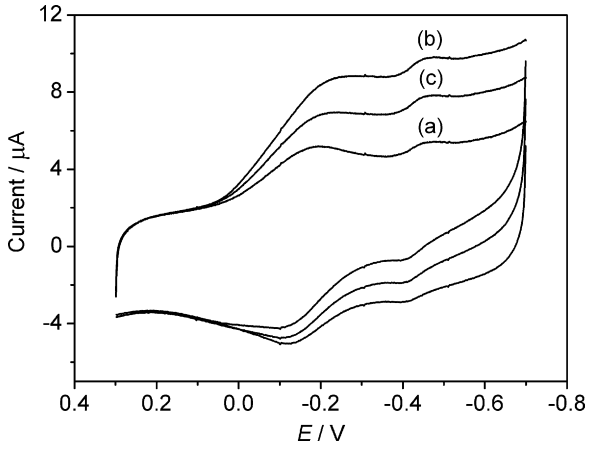

Fig. 5. Cyclic voltammograms of AOx/CNF–FeTMPyP modified GCE in nitrogen-saturated (a) and air-saturated (b) pH 7.0 PBS, and air-saturated pH 7.0 PBS containing 10 mM ethanol (c). Scan rate: 0.05 V s^{-1}.

tion current was also maximum, indicating a saturated coverage of CNF by FeTMPyP. On the other hand, when 5 mg CNF was mixed to 1.0 ml FeTMPyP solution, with the decreasing FeTMPyP concentration from 2 mg ml^{-1}, the reduction current decreased. When the FeTMPyP concentration was higher than 2 mg ml^{-1}, more free FeTMPyP could be monitored by UV–vis absorption at 422 nm^{-1}. Thus 2 mg ml^{-1} FeTMPyP solution with 5 mg CNF for 1.0 ml FeTMPyP solution was used for the preparation of CNF–FeTMPyP nanocomposite.

The amount of FeTMPyP adsorbed on the CNF–FeTMPyP modified electrode could be evaluated from the anodic or cathodic peak area of $Fe^{(III)}$TMPyP/$Fe^{(II)}$TMPyP redox couple. The value was estimated to be 4.5×10^{-9} mol cm^{-2}, which was larger than those of 2.7×10^{-9} mol cm^{-2} hemin/MWNTs modified electrode (Ye et al., 2004), and much larger than the monolayer coverage of FeTMPyP molecules. This was obviously due to a mass of FeTMPyP molecules in the hybrid nanocomposite.

3.3. Amperometric sensing of dissolved oxygen

Fig. 4 displays the steady-state amperometric response of the CNF–FeTMPyP modified electrode to dissolved oxygen at an optimal applied potential of −0.20 V. The current–time curve clearly illustrated that the modified electrode could respond very rapidly to the change in the O_2 concentration, producing steady-state signals within 5 s. The response displayed a linear O_2 concentration range from 6.5 nM to 6.4 μM with a correlation coefficient of 0.999 and a slope of 714.7 nA μM^{-1}. The limit of detection was 1.1 nM at the signal to noise ratio of 3. The high sensitivity came from the synergy effect of CNF and FeTMPyP in the biofunctional nanocomposite to accelerate the reduction of dissolved oxygen at low reduction potential. Repeated use of the electrodes did not affect the long-term stability. The coefficients of variation of the current signals for eight repeated injections of 0.05 and 1 μM O_2 were 7.4% and 2.7%, respectively. The oxygen biosensor showed acceptable preparation reproducibility with a relative standard deviation of 6.8% estimated from the slopes of the calibration plots at six freshly prepared CNF–FeTMPyP modified electrodes. No obvious decrease in the response to O_2 was observed after three months of storage.

3.4. Amperometric biosensing of ethanol

Based on the highly catalytic activity and biocompatibility of the CNF–FeTMPyP hybrid nanocomposite, an ethanol biosensor was fabricated by further immobilizing AOx with PVA to the surface of CNF–FeTMPyP modified electrode. The resulting modified electrode showed two couples of stable and well-defined redox peaks (Fig. 5). The redox peaks located at couple of −0.189 and −0.117 (ΔE_p = 72 mV) were also attributed to the direct electron transfer between FeTMPyP and electrode. The slightly increasing peak-to-peak separation was due to the presence of PVA, which slowed the electron transfer rate. Interestingly, the electrode showed the direct electrochemistry of AOx with the redox potentials of −0.408 V and −0.464 V, which has never been directly observed probably due to steric hindrances and large reaction barriers (Azevedo et al., 2005). Thus CNF provided a microenvironment for preserving the natural structure and accelerating the electron transfer of the immobilized redox proteins. The ratios of reduction to oxidation peak currents of the two couples of peaks were about 1:1 in oxygen-free PBS, furthermore, the peak currents increased linearly and the peak potentials showed a small shift with the increasing scan rate from 10 mV s^{-1} to 100 mV s^{-1}, indicating two surface-controlled electrode processes.

Almost all AOx-based ethanol amperometric sensors developed so far are based on the monitoring of O_2 consumption at −600 mV or H_2O_2 formation at +600 mV in AOx enzymatic cycle. This work was also based on monitoring O_2 consumption with AOx/CNF–FeTMPyP modified electrode. Firstly ethanol was selectively oxidized by oxygen in AOx enzymatic cycle, which decreased the oxygen concentration. And then the O_2 consumption was monitored by the electrochemical signal of oxygen reduction at CNF–FeTMPyP modified sensor surface. The excellent catalytic activity of both CNF and FeTMPyP toward the reduction of dissolved oxygen and good selectivity of AOx resulted in highly selective and sensitive amperometric response to ethanol at a low overpotential of oxygen reduction. The low reduction potential was an advantage for excluding the interference of other coexisted species.

As shown in Fig. 6, upon additions of ethanol aliquots to static air-saturated pH 7.0 PBS the chronoamperometric curves showed decreasing response. The current reached quickly the steady value, the time reaching 95% of the steady value was less than 10 s, which was much faster than those of 120 s at AOx/gelatin modified electrode (Akyilmaz and Dinçkaya, 2005) and 30–50 s at AOx/polvinylferrocenium modified electrode (Gülce et al., 2002), as shown in Table S1 in supporting information. The biosensing response decreased linearly in the ethanol concentration range from 2.0 μM to 112 μM. The sensitivity was 1.93 nA μM^{-1} with a detection limit of 1.2 μM, which was much lower than those (Table S1 in supporting information) of 30 μM for AQx/chitosan

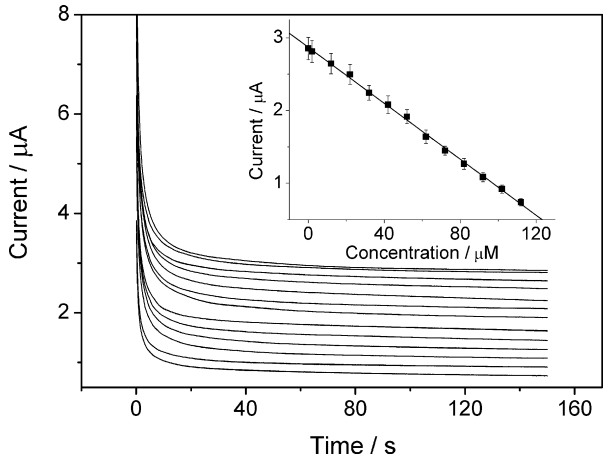

Fig. 6. Chronoamperograms of AOx/CNF–FeTMPyP/GCE in air-saturated 0.2 M pH 7.0 PBS containing 0, 2, 12, 22, 32, 42, 52, 62, 72, 82, 92, 102 and 112 μM ethanol (from top to bottom). Inset: Linear calibration curve.

at an eggshell membrane-based biosensor with response time of 60 s (Wen et al., 2007) and 80 μM for graphite–teflon composite bienzyme amperometric biosensor with response time of 115 s (Guzmán-Vázuez de Prada et al., 2003), and 540 μM for microseparation chips based on performing multienzymatic dehydrogenase/oxidase assays (Wang et al., 2001). The detection limit was also lower than that obtained at alcohol dehydrogenase/CNF modified electrode by monitoring the electrocatalytic oxidation current of NADH (Wu et al., 2007a). More importantly, the detection process had no the need of stirring, which is advantageous for in situ monitoring of ethanol.

Since the biofunctional CNF–FeTMPyP modified electrode provided the advantage for detecting oxidase substrate at a low reduction potential (−0.2 V vs. SCE), some common interference such as ascorbic acid and lactic acid (as antioxidants), citric acid, acetic acid and cane sugar (as flavorings) in real samples could be excluded. At 200 μM interferents, the decrease in O_2 consumption were equivalent to those of 4.1 ± 0.03, 1.5 ± 0.01, 2.9 ± 0.02, 1.1 ± 0.01, 1.7 ± 0.02 μM of ethanol (Table S2 in supporting information), respectively, showing slight interferences. The much lower concentrations of these interferents than ethanol in usual samples such as beers and liquors indicates good practicability of the biosensor. The analysis of ethanol was carried out in beer without any need of sample pretreatment except a dilution step. The concentration of ethanol in beer was determined to be 0.70 M or 4.14% (v/v), which was consistent with the given value of ≥4.0% (v/v). The recovery tests were performed by adding 20 μM and 80 μM ethanol to the beer sample, which produced the recovery of 110 ± 1.7 and 106 ± 2.0% (Table S3 in supporting information), demonstrating good accuracy for the determination of ethanol in real sample.

The coefficients of variation for intra-assay with six measurements using this biosensor were 4.5% and 3.6% at ethanol concentrations of 10 μM and 80 μM, respectively. In addition, the relative standard deviation of current signals for measurement of 20 μM ethanol at six independently prepared biosensors was 7.9%, which proved good reproducibility of the biosensor preparation.

The stability of the AOx/CNF–FeTMPyP modified electrode was investigated when stored in 0.2 M pH 7.0 PBS at 4 °C and measured at intervals over several days. No obvious decrease in the response to ethanol was observed after 20 days of storage. After 30 days the response current was still retained at 91% value of the initial response. This implied that the three-dimensional structure of the AOx/CNF–FeTMPyP membrane was very efficient for retaining the bioactivity of ethanol oxidase and preventing it from leaking out of the sensor.

4. Conclusions

A biofunctional nanocomposite of CNF–FeTMPyP was conveniently prepared through π–π non-covalent interaction without any treatment. The hybrid nanocomposite possesses good dispersion in water and accelerates the electron transfer of FeTMPyP at electrode. Both the FeTMPyP and CNF in the nanocomposite prompt the electron transfer between dissolved oxygen and electrode and show a synergic effect in electrocatalysing the reduction of oxygen. The nanocomposite realizes for the first time the direct electron transfer of AOx. Based on the excellent electrocatalytic activity toward oxygen reduction, a biosensor for ethanol was constructed by immobilizing AOx on CNF–FeTMPyP modified electrode. The biosensor shows rapid and highly sensitive amperometric response to ethanol at a low reduction potential without need of stirring. Thus, the hybrid nanocomposite of carbon nanofiber with water-soluble porphyrin provides an attractive insight as a functional electrocatalyst to construct sensitive biosensor and mimic the catalytic behaviors of enzyme in biological systems.

Acknowledgements

This project was supported by the funds for Creative Research Groups (20521503), Major Research Plan (90713015), Key Program (20535010) and General Program (20745003, 20705012) from NNSFC, PhD Fund of MOE for Young Teachers (20070284052) and the Science Foundation of Jiangsu (BK2007570).

Appendix A. Supplementary data

Supplementary data associated with this article can be found, in the online version, at doi:10.1016/j.bios.2008.06.009.

References

Akyilmaz, E., Dinçkaya, E., 2005. Biosens. Bioelectron. 20, 1263–1269.
Azevedo, A.M., Prazeres, D.M.F., Cabral, J.M.S., Fonseca, L.P., 2005. Biosens. Bioelectron. 21, 235–247.
Balaban, T.S., Linke-Schaetzel, M., Bhise, A.D., Vanthuyne, N., Christian, R., Anson, C.E., Buth, G., Eichhöfer, A., Foster, K., Garab, G., Gliemann, H., Goddard, R., Javorfi, T., Powell, A.K., Rösner, H., Schimmel, T., 2005. Chem. Eur. J. 11, 2267–2275.
Bard, A.J., Faulkner, L.R., 2001. Electrochemical Methods: Fundamentals and Application, 2nd ed. Wiley, New York.
Bedioui, F., Bouhier, Y., Sorel, C., Devynck, J., Coche-Guerente, L., Deronzier, A., Moutet, J.C., 1993. Electrochim. Acta 38, 2485–2491.
Boujtita, M., Hart, J.P., Pittson, R., 2000. Biosens. Bioelectron. 15, 257–263.
Boultatov, R., Collman, J.P., Shiryaeva, I.M., Sunderland, C.J., 2002. J. Am. Chem. Soc. 124, 11923–11935.
Chen, J., Collier, C.P., 2005. J. Phys. Chem. B 109, 7605–7609.
Chen, R.J., Zhang, Y., Wang, D., Dai, H., 2001. J. Am. Chem. Soc. 123, 3838–3839.
Collman, J.P., Boulatov, R., Sunderland, C.J., Fu, L., 2004. Chem. Rev. 104, 561–588.
Cui, H., Kalinin, S.V., Yang, X., Lowndes, D.H., 2004. Nano. Lett. 4, 2157–2161.
Gülce, H., Gülce, A., Kavanoz, M., Coşkun, H., Yıldız, A., 2002. Biosens. Bioelectron. 17, 517–521.
Guldi, D.M., Rahman, G.M.A., Zerbetto, F., Prato, M., 2005. Acc. Chem. Res. 38, 871–878.
Guzmán-Vázuez de Prada, A., Peña, N., Mena, M.L., Reviejo, A.J., Pingarrón, J.M., 2003. Biosens. Bioelectron. 18, 1279–1288.
Hao, C., Ding, L., Zhang, X., Ju, H.X., 2007. Anal. Chem. 79, 4442–4447.
Hasobe, T., Fukuzumi, S., Kamat, P.V., 2005. J. Am. Chem. Soc. 127, 11884–11885.
Hasunuma, T., Kuwabata, S., Fukusaki, E., Kobayashi, A., 2004. Anal. Chem. 76, 1500–1506.
Jang, J., Bae, J., Choi, M., Yoon, S.H., 2005. Carbon 43, 2730–2736.
Lei, J.P., Ju, H.X., Ikeda, O., 2004a. Electrochim. Acta 49, 2453–2460.
Lei, J.P., Ju, H.X., Ikeda, O., 2004b. J. Electroanal. Chem. 567, 331–338.
Li, X.F., Fu, Y.Q., Sun, C.Q., 2003. Electroanalysis 15, 1707–1712.
Liu, Y., Yan, Y.L., Lei, J.P., Wu, F., Ju, H.X., 2007. Electrochem. Commun. 9, 2564–2570.
Murakami, H., Nomura, T., Nakashima, N., 2003. Chem. Phys. Lett. 378, 481–485.

Pasternack, R.F., Lee, H., Malek, P., Spencer, C., 1977. J. Inorg. Nucl. Chem. 39, 1865–1870.
Salimi, A., MamKhezri, H., Hallaj, R., Zandi, S., 2007. Electrochim. Acta 52, 6097–6105.
Takagi, S., Eguchi, M., Tryk, D.A., Inoue, H., 2006. J. Photochem. Photobio. C: Photochem. Rev. 7, 104–126.
Vamvakaki, V., Tsagaraki, K., Chaniotakis, N., 2006. Anal. Chem. 78, 5538–5542.
Wang, J., Chatrathi, M.P., Tian, B., 2001. Anal. Chem. 73, 1296–1300.
Wasser, I.M., Huang, H., Moënne-Loccoz, P., Karlin, K.D., 2005. J. Am. Chem. Soc. 127, 3310–3320.
Wen, G., Zhang, Y., Shuang, S., Dong, C., Choi, M.M.F., 2007. Biosens. Bioelectron. 23, 121–129.
Wu, X.J., Choi, M.M.F., 2004. Anal. Chem. 76, 4279–4285.
Wu, L.N., Zhang, X.J., Ju, H.X., 2007a. Anal. Chem. 79, 453–458.
Wu, L.N., Zhang, X.J., Ju, H.X., 2007b. Biosens. Bioelectron. 23, 479–484.
Ye, J.S., Wei, Y., Zhang, W.D., Cui, H.F., Gan, L.M., Xu, G.Q., Sheu, F.S., 2004. J. Electroanal. Chem. 562, 241–246.
Yıldız, H.B., Toppare, L., 2006. Biosens. Bioelectron. 21, 2306–2310.
Zenkevich, E., Cichos, F., Shulga, A., Petrov, E.P., Blaudeck, T., von Borczyskowski, C., 2005. J. Phys. Chem. B 109, 8679–8692.